Astron. Nachr. / AN **???**, No. ???, 1 – 15 (2007) / **DOI *please set DOI!***

The inner structure of the S0 galaxy NGC 3384

H. Meusinger[1,⋆], **H. A. Ismail**[2], and **P. Notni**[3,⋆⋆]

[1] Thüringer Landessternwarte, Sternwarte 5, D-07778 Tautenburg, Germany
[2] National Research Institute of Astronomy and Geophysics, Cairo, Egypt
[3] Leo-Sachse-Str.97, 07749 Jena, Germany

Received 28 Dec 2006, accepted 30 Jan 2007
Published online later

Key words galaxies: peculiar – galaxies: individual (NGC3384) – galaxies: structure – galaxies: evolution

We re-investigate the lenticular galaxy NGC 3384, a member of the Leo I galaxy group, using *HST* and multi-colour Calar Alto observations. Various approaches are used to visualize the two known peculiar components, the so-called inner component (IC) and the elongated component (EC), on the *HST* images. The methods were checked in detail using synthetical images from simulated galaxies. For the first time, we make the IC as well as the inner part of the EC visible on direct images. The results confirm both the bar-like appearance of the inner EC and the quasi-elliptical shape of the IC. The IC resembles an inclined disk where the surface brightness becomes successively shallower towards the centre compared to an exponential profile. The orientation of the inner part of the EC is perpendicular to the major axis of the IC. The broad-band colour indices are shown to be in agreement with model predictions for a 5 to 7 Gyr old stellar population of quasi-solar metallicity. No significant large-scale variations of the colour indices over the main body of the galaxy are found. We discuss the previously reported colour gradients close to the nucleus and argue that the most plausible explanation is reddening by small amounts of dust though unsharpe masked *HST* images do not provide significant hints for clumpy dust. According to the episodic dust settling scenario suggested by Lauer et al (2005), the very low dust fraction indicates that NGC 3384 is in a post-activity phase and at the beginning of a new dust-settling cycle.

1 Introduction

NGC 3384 is an apparently unspectacular yet fascinating "classical" S0 galaxy in the nearby galaxy group Leo I. Its appearance on a photographic plate was described by Pease (1920) as "an astonishing nebula consisting of a bright center $40''$ diameter, on which are superimposed a very bright elongated nucleus $19'' \times 10'', p\ 45°$, crossed by a second bright nucleus $40'' \times 5'', p\ 130°$, presenting a Saturn-like appearance". Since that time, NGC 3384 was a target of a variety of photometric, spectroscopic, and kinematic studies of samples of nearby early-type galaxies (e.g., Fisher 1997; Pinkney et al. 2003; Emsellem et al. 2004; Erwin 2004; Lauer et al. 2005; Sil'chenko 2006). Early-type galaxies are now known to exhibit a rich variety of distinct morphological features like e.g., twisted and/or non-concentric isophotes, disky or boxy deviations of the isophotes from pure ellipses (Lauer 1985), outer shells (Malin & Carter 1983), pseudo-bulges (Kormendy & Kennicutt 2004), double bars (Erwin 2004), and supermassive central black holes (Kormendy & Richstone 1995).

All these peculiar features have been identified in NGC 3384: strong isophote twist and centre position variation (Barbon et al. 1976), outer boxy and inner disky isophotes (Busarello et al. 1996); a faint extended luminous arc (outer shell) at the N-E side and outside the main galaxy was first discovered by Malin (1984) from a photographically amplified image and is clearly indicated also on the blue POSS II image. NGC 3384 was classified by Pinkney et al (2003) as a possible pseudo-bulge galaxy and by Erwin (2004) as a bar-in-bar galaxy. The dynamically derived mass of the central black hole is $1.6\,10^7 \mathrm{m}_\odot$ (Tremaine et al 2002). Finally, we note that NGC 3384 is one of the only two galaxies were a new class of extended star clusters known as "faint fuzzies" were detected so far (Burkert et al 2005).

The interest in such morphological peculiarities is mainly motivated by the fact that they are tracers of the past galaxy evolution, either rapid evolution driven by mergers (Toomre & Toomre 1972) or slow, secular evolution driven by other external or internal processes (Kormendy & Kennicutt 2004). NGC 3384 is a good example for the investigation of such processes in the relatively poor galaxy environment of a loose galaxy group. A past collision of NGC 3384 with NGC 3368 was suggested by Rood & Williams (1985) whereas the detailed study of the Leo I group galaxies by Sil'chenko et al (2003) suggests that many of their properties are in line with the scenario of tidal interactions of the galaxies with a supergiant intergalactic ring of HI clouds.

A detailed study of NGC 3384 was presented by Busarello et al (1996) where also a comprehensive summary of its basic properties can be found. Their investigation was

⋆ Corresponding author: e-mail: meus@tls-tautenburg.de

⋆⋆ Visiting astronomer, German-Spanish Astronomical Center, Calar Alto, operated by the MPIA, Heidelberg, jointly with the Spanish National Commission for Astronomy.

based on imaging and spectroscopy from ground-based telescopes, including the ESO NTT. The NTT image, processed with an adaptive filter, revealed the existence of an hitherto unknown, small ($r \sim 6''$) central component aligned to the major axis of the galaxy ($PA \approx 46°$). This is called by of Busarello et al the *inner component* (IC). Kinematical data from long-slit or integral-field spectroscopy are in line with the interpretation of the IC as a very rapidly rotating component which is kinematically colder than the surrounding (Busarello et al 1996; Fisher 1997; Sil'chenko et al 2003; Emsellem et al 2004). The previously known almost peanut-shaped *elongated component* (EC), at position angle $PA \approx 132°$, is probably best interpreted as a bar. The EC has been known for a long time (Pease 1920). For the IC, on the other hand, no direct image was extracted so far due to its small size and intrinsic faintness.

Busarello et al mentioned that their re-investigation of NGC 3384 was relying on the rule "that it is far easier to see something when it is known to be there". Following the same rule, the present paper is aimed mainly at the visualization of the IC and the discussion of its properties based on new, high-resolution images. A second aim is to characterize the stellar population in the galaxy by the comparison of colour indices from multi-colour photometry with population synthesis models.

The paper is organized as follows. First, we give a brief overview over the observational data in Sect. 2, than we present large-scale light profiles in Sect. 3. In Sect. 4, we analyze the structures in the inner $\sim 15''$ on *HST* images. Sections 5, 6, and 7 deal with the comparison of the colour data with evolution models and the possible presence of dust and, finally, the conclusions. Throughout this paper we assume a distance of $d = 11.7$ Mpc (Tonry et al 2001), corresponding to a scale of 56.7 pc per arcsec.

2 Observational data

Whereas the study of the small-scale structure in the centre of the galaxy clearly requires high spatial resolution, the sky background correction is essential for the investigation of the colour distribution. Lauer et al (2005) have measured a pseudo-sky level from the corner of the WFPC2 WF3 CCD at a distance of about $1\farcm8$ from the centre i.e., still within the galaxy. A major aim of the present study is to derive ages of the galaxy components from the projected distribution of colours. The results are very sensitive to the photometric calibration and in particular to the correct sky background subtraction. Therefore, the field of view must be larger than the angular size of the galaxy which is about $5\farcm5 \times 2\farcm5$.

For the study of the colour distribution in NGC 3384 we prefer ground-based observations with a sufficiently large field of view, despite a poorer spatial resolution. CCD observations were obtained by one of us (P.N.) in February 1995 using the 1.23 m telescope on Calar Alto, equipped with a TEK CCD camera with 1024×1024 pixels of 24μm$\times$ 24μm. The field of view amounts to $8\farcm5 \times 8\farcm5$ with an image scale of $0\farcs502$ pixel^{-1}. Images were taken through Johnson-Cousins B, V, R and I filters with typically two or more exposures per filter. Typical exposure times are 1 500 s U, 500 s B, 300 s V, 100 s R, and 100 s I. The sky conditions were good, the seeing varied between $1''$and $2''$. Flatfields were obtained during morning and evening twilight, from which a master flat has been made.

The bias-corrected and flatfielded frames were matched carefully in position using the foreground stars in the field, and transformed to a common coordinate system. Cosmics were eliminated as usual by interpolation between neighbouring pixels. A similar procedure was used to clean the image from bright foreground stars for precise surface photometry. Finally, all images from the same filter band were co-added to produce one final image per band. All image reductions have been conducted using standard procedures from the ESO MIDAS image processing package.

High resolution images of the inner part of NGC 3384 are available from the data archives. *Hubble Space Telescope (HST)* images were taken in 1995 with the planetary camera CCD in WFPC2 (PI: T. Lauer; see Lauer et al 2005). The field of view amounts to $36'' \times 36''$ with an image scale of $0\farcs0456$ px^{-1}, corresponding to 2.58 pc px^{-1} at the distance of NGC 3384. Three exposures were taken in each of the filter bands F555W and F814W, equivalent to broadband V and I, respectively with 350 s per exposure. Hence, cosmic-ray event repair could be done easily by the comparison of the frames from the same filter band. In addition, we use on-the-fly-reprocessed ACS/HRC images, taken in June 2005 (PI: R. O'Connell), downloaded from the Multimission Archive at STScI (MAST). The exposure times are 2552 s, 1912 s, and 432 s, respectively, for the three filters F250W, F330W, and F555W. At higher energies ($0.3 \ldots 8$ keV), a 10 ks *CHANDRA* event file, taken in Oct. 2004 (PI: Y. Terashima) with the S-array of the Advanced CCD Imaging Spectrometer (ACIS), is available from the *CHANDRA* Data Archive; the pixel scale is $0\farcs492$ px^{-1}.

3 Global properties from the BVR surface photometry

In this Section, we use the UBVR frames from Calar Alto because they cover the whole galaxy. Each frame was thoroughly background-corrected before a final image per filter band was produced. The brightness of the sky background in each frame was estimated using polynomials of second order for the "average" value in selected background areas. The areas are chosen via small boxes distributed over the outskirts of the frames. Then an average image for each filter is obtained. A convenient compilation of aperture photoelectric magnitudes of galaxies is published by Prugniel & Heraudeau (1998), which have been used here to transform our instrumental magnitudes to the standard Johnson-Cousins system. The rms error values of our photometric

zero points in B, V, R and I are 0.03, 0.01, 0.02 and 0.01 mag, respectively.

The quantitative analysis of the surface photometry was obtained by fitting the isophotes of the galaxy with concentric ellipses using the task ELLIPSE of the ISOPHOTE package in IRAF. The task reads the two-dimensional image and produces a table containing the essential parameters for each fitted isophote such as the brightness level, ellipticity, position angle, etc. The table content is used later on as input in the IRAF task BMODEL to reconstruct a galaxy image with perfect elliptical and concentric isophotes.

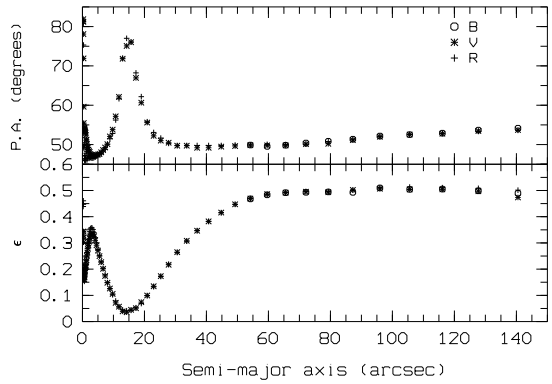

Fig. 1 The change of the position angle (top) and the ellipticity (bottom) with the semi-major axis in the B, V, and R band.

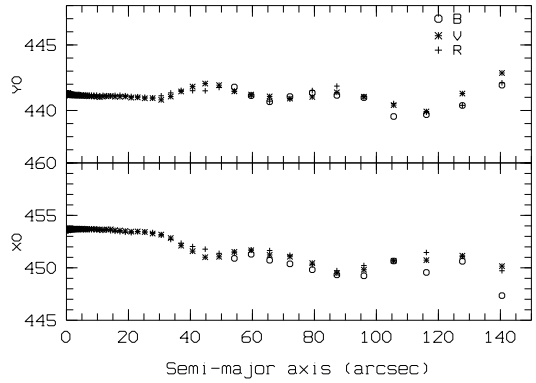

Fig. 2 The drift of the centre coordinates (pixels).

The results based on the ellipse fitting are shown in Fig.s 1 to 3. Figure 1 gives the variation of the position angle and the ellipticity $\epsilon = 1 - b/a$, where a and b are the semi-major axis and the semi-minor axis, respectively, as a function of a. The ellipticity has a local maximum at $a \approx 3''$ where the position angle reaches a minimum, and vice versa the maximum of the position angle at $a \approx 15''$ corresponds to a minimum of the ellipticity. The same features have been reported already by Busarello et al (1996) in the B and R

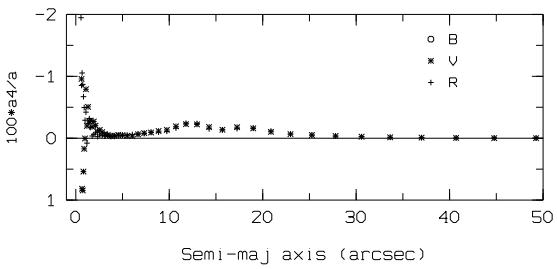

Fig. 3 The change of the normalized Fourier parameter a_4/a.

bands and by Sil'chenko et al (2003) in the JHK bands. The estimated mean values ($\pm$ standard deviation) of the ellipticity and the position angle at $a = 50''$ are $\epsilon_{50} = 0.49$ and $PA_{50} = 50.6°$, respectively, in perfect agreement with Busarello et al and Sil'chenko et al. These authors interpreted the local maximum of the ellipticity in the inner region ($a \approx 5''$) as due to the presence of the IC. The minimum of the ellipticity and the corresponding maximum of the position angle at $a \approx 15''$ is assigned to the superposition of a flattened spheroid, $PA \approx 50°$, with the EC which is elongated almost along the minor axis.

The variation of the centres of the isophotes is shown in Fig. 2 where $x0, y0$ increase toward W and N, respectively. Again, the general trend is similar to the results shown by Busarello et al. Especially, we establish their finding that the drift of the isophote centre is very small within the region of the EC ($\lesssim 25''$ along the minor axis). At larger distances, the isophote centres shift toward NE, opposite to the position of the neighbour galaxy NGC 3379, indicating the large-scale asymmetry discussed by Busarello et al. The finding that there is also a NE shift at $\sim 110 \ldots 140''$ is original to the present paper.

Low-order deviations of the isophotes from perfect ellipses are quantified by the fourth order Fourier harmonics a_4 with $a_4 > 0$ for disky and $a_4 < 0$ for boxy isophotes. The boxy shape of NGC 3384 is clearly seen at $a \approx 10'' \ldots 20''$ in Fig. 3. A disky inner structure is marginally indicated in the B image at $a \approx 3''$.

4 Inner substructure

4.1 Surface photometry

For the analysis of the inner substructure we started with the PC part of the *HST* WFPC2 images. Following Lauer et al (2005), we first deconvolved the PSF using the Lucy-Richardson algorithm (MIDAS procedure DECONVOLVE/ FLUCY). Except for some reddening ($\Delta(V-I) \approx 0.1$ mag towards the centre within the innermost $10''$, see also Lauer et al (2005, their Fig. 3), the images in the F555W filter and the F814W filter are very similar. Therefore, we decided to co-add both frames to get a deeper combined image with increased signal-to-noise ratio in the outer parts. In addition,

the *HST* ACS images were analyzed in a similar way but without co-adding the frames from the three different filter bands.

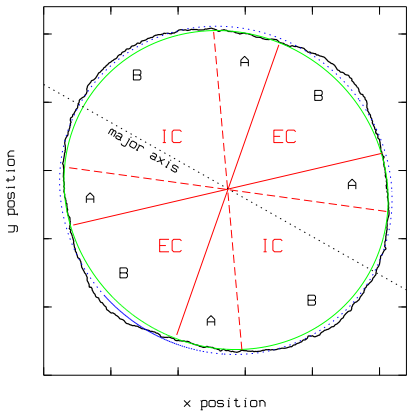

Fig. 4 A single outer isophote from the PC part of the *HST* WFPC2 image (thick curve) clearly showing deviations from ellipticity due to the "inner component" (IC) and the "elongated component" (EC). Best fitting ellipses are shown as dotted curve (EF = ellipse fitting to the whole isophote) and solid curve (IEF = *inner* ellipse fitting, i.e. in the angular intervals between IC and EC only), respectively. The direction of the major axis of the fitting ellipse ($a = 11\farcs2$, PA$= 60°$) is indicated by the dotted line. For the meaning of the labels "A" and "B" see Sect.4.2.

The isophote plot in Fig.6 indicates a boxy shape in the outer part and a disky shape in the inner part in agreement with the Fourier coefficient a_4 from the Calar Alto images (Fig. 3; see also Busarello et al 1996). According to Lauer (1985), boxies are described by "pulling the isophote in towards the centre of the galaxy on the major and minor axes, but pushing it out 45° in between". The closer inspection of the isophotes (see Fig. 4) reveals that their shape is slightly different from pure boxies in the sense of Lauer. It is reasonable to interpret the isophote shape seen in Fig. 4 as due to the superposition of the IC and the EC. A disky inner structure, caused by the IC, is indicated by weak ansae at $PA \approx 47°$. Though not conspicuous in the contour plot in Fig. 6, they are clearly indicated by the results of the ellipse fit at $a \approx 3 \ldots 6''$. For the EC, with a diameter of about $20''\ldots40''$, only the inner part is covered by the field of the planetary camera CCD.

In Fig. 5, we plot the surface photometry for the inner $10''$ on the *HST* ACS F555W image. As the style of the presentation is similar to the surface photometry given by Lauer et al (2005) for the *HST* WFPC2 F555W image, the perfect agreement with their results is easily recognizable. The IC is indicated by the noticeable increase of the ellipticity between $a \approx 0.2''$ and $5''$ with a maximum $\epsilon_{max} = 0.44$, i.e. $\sim 10\%$ higher than in the NTT image from Busarello et al. At small distances from the centre ($a \lesssim 0\farcs1$), the nucleus

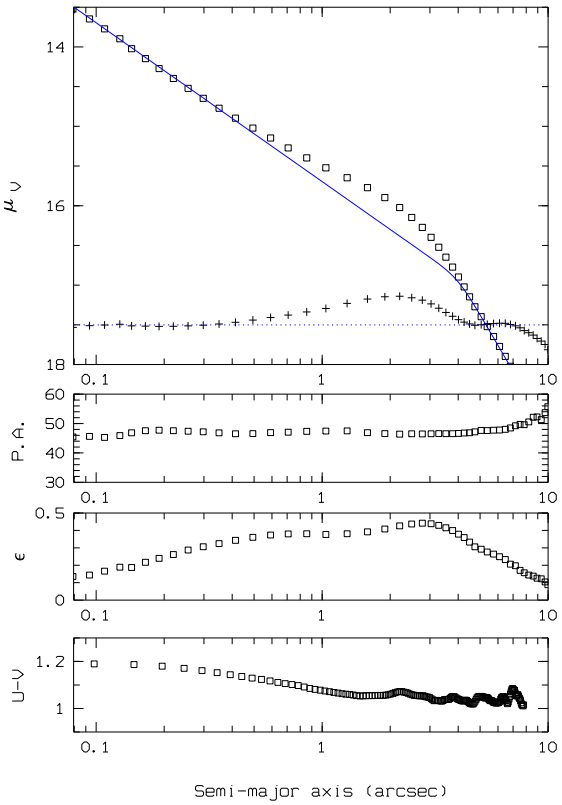

Fig. 5 Surface photometry for the *HST* ACS F555W filter. The style is similar to that in Lauer et al (2005). The solid line in the top panel is the Nuker law fitted to the brightness profile; the trace of the bottom of the panel (crosses) shows the residuals from the fit (the dotted line indicates the zero level). The next panels give the isophote position angle, the ellipticity $\epsilon = (1 - b/a)$, and the colour index $U - V$ as functions of semi-major axis. The colour index is measured in a $1''$ wide strip along the major axis. As in Lauer et al, no Galactic absorption correction has been applied.

is dominating. From the shape of the isophotes (Fig. 6), we conclude that the EC becomes important only at large distances ($r \gtrsim 10''$ along the minor axis).

It is well known that the inner surface brightness profiles of early-type galaxies can be approximated by a Nuker law (Lauer et al. 1995), which consists essentially of two different power laws. In particular, the Nuker fit is useful to distinguish between power-law galaxies and core galaxies (Lauer et al. 2005). NGC 3384 is clearly characterized as a power-law galaxy by the Nuker fit, though the fit shown by Lauer et al is obviously not perfect (as, however, for other galaxies too). We find it tempting to speculate that the deviations might be caused by the IC. In Fig. 5 we show a Nuker fit with parameters different from those given by Lauer et al. (2005) but providing a good fit for the distance range where the IC is not dominating. The residuals from this fit show indeed a nice correlation with the ellipticity, as expected if the residuals are dominated by the IC.

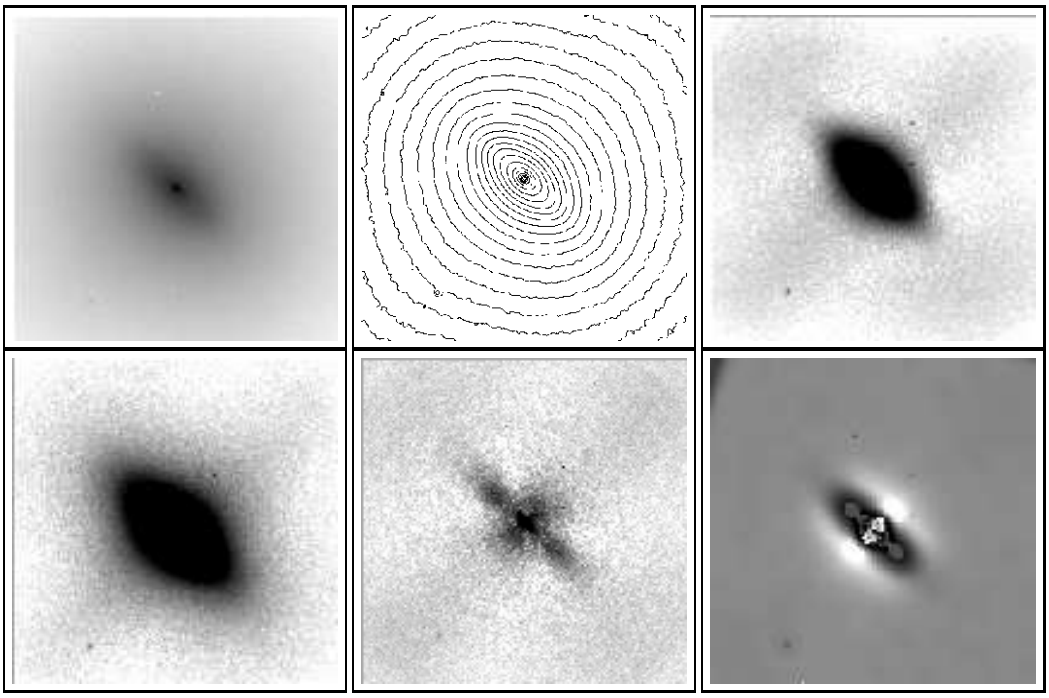

Fig. 6 Inverse logarithmic grey-scale presentation of the combined *HST* planetary camera image of NGC 3384. *Top, left to right*: (a) original image, (b) contour plot, (c) residual image after subtraction of the profile fitting model. *Bottom, left to right*: residual images after subtraction of the corresponding model image derived from (d) unsharp masking, (e) inner ellipse fitting (IEF). (f) result from adaptive Laplace-filtering. Image size $24'' \times 24''$ (corresponding to 1.36 kpc at the distance of NGC 3384). N up, E left.

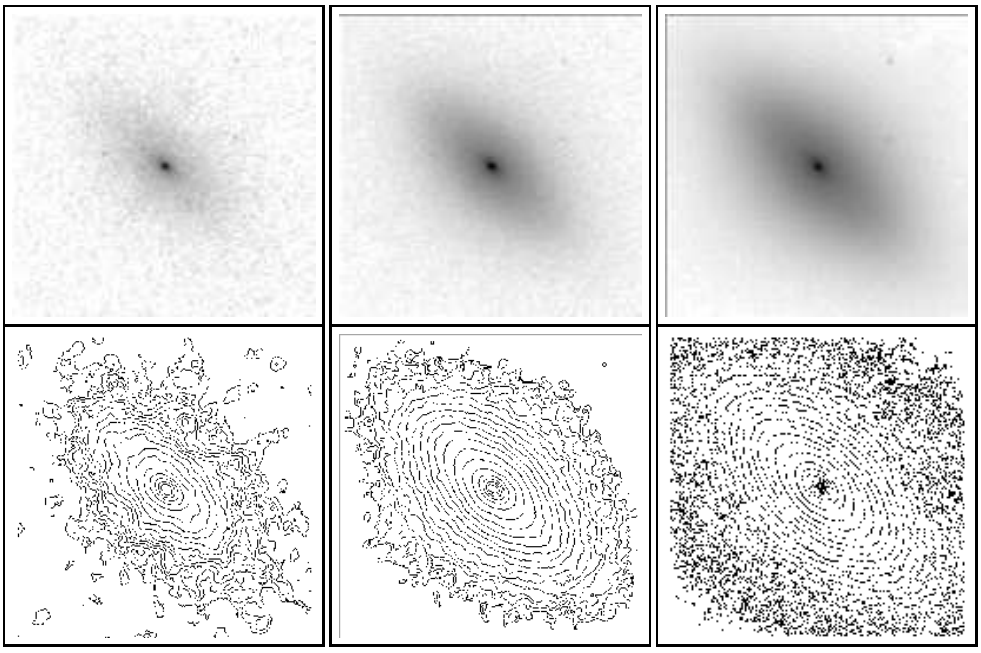

Fig. 7 *Top:* the inner $12'' \times 12''$ region of NGC 3384 after subtraction of the median-filtered *HST* ACS images in the F250W, F330W, and F555W filter band (left to right). The intensity interval is the same, N up, E left. *Bottom:* corresponding contour plots (see text).

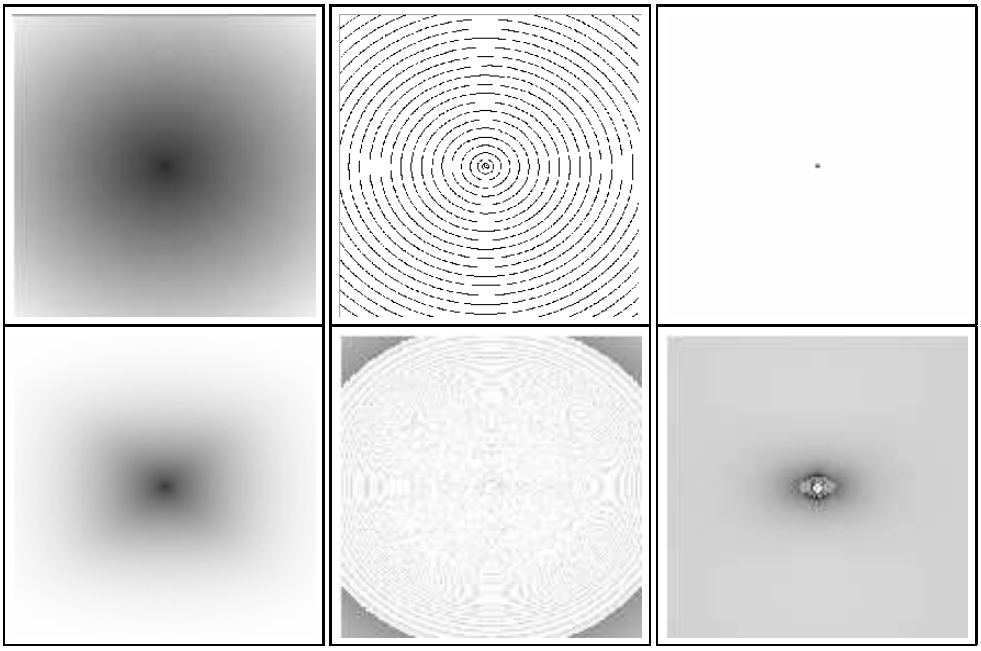

Fig. 8 Inverse logarithmic grey-scale presentation of model **DBN**. *Top, left to right:* (a) all components, (b) contour plot of image (a), (c) components without disk and bulge (upper right). *Bottom, left to right:* (d) residual image after subtraction of the median-filtered image, and (e) residual image after subtraction of the corrected IEF model. (f) adaptive Laplace-filtered image. Same scale for all images.

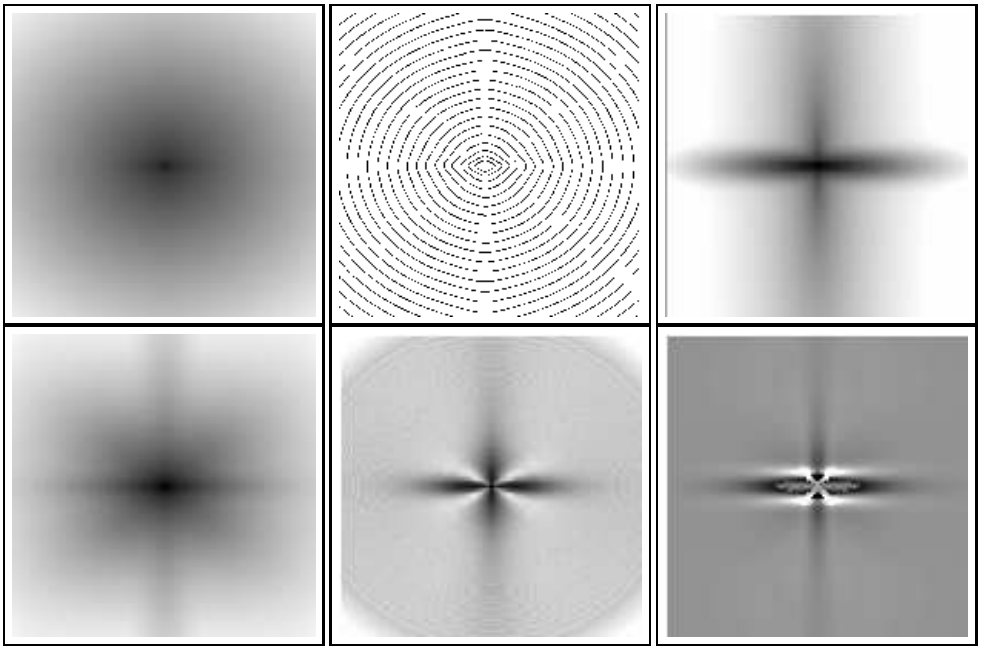

Fig. 9 As Fig.9, but for model **DBNEI**$_1$.

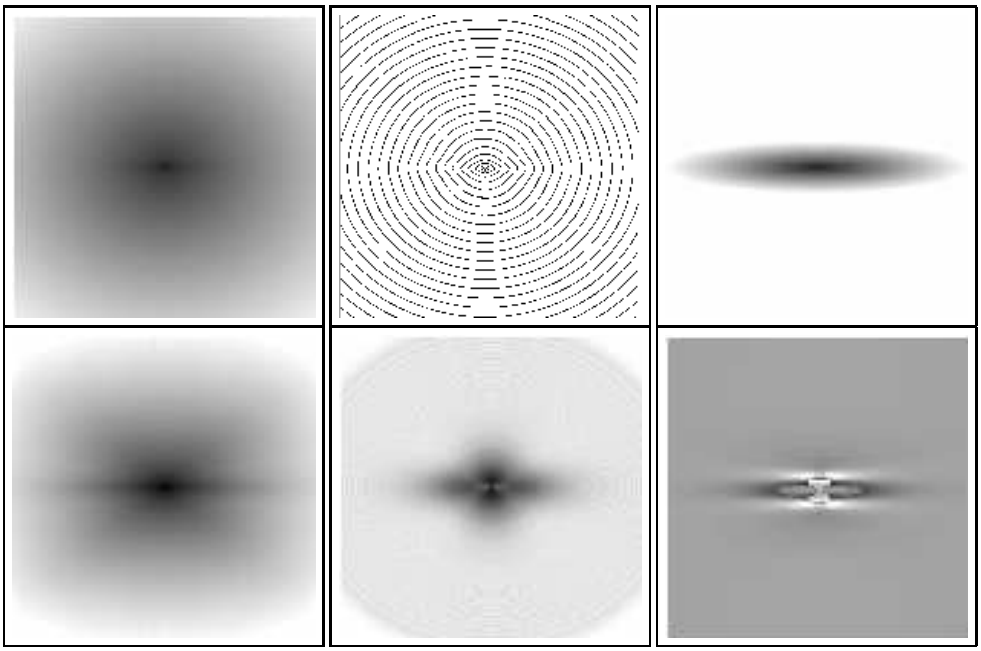

Fig. 10 As Fig.9, but for model **DBNI**$_1$.

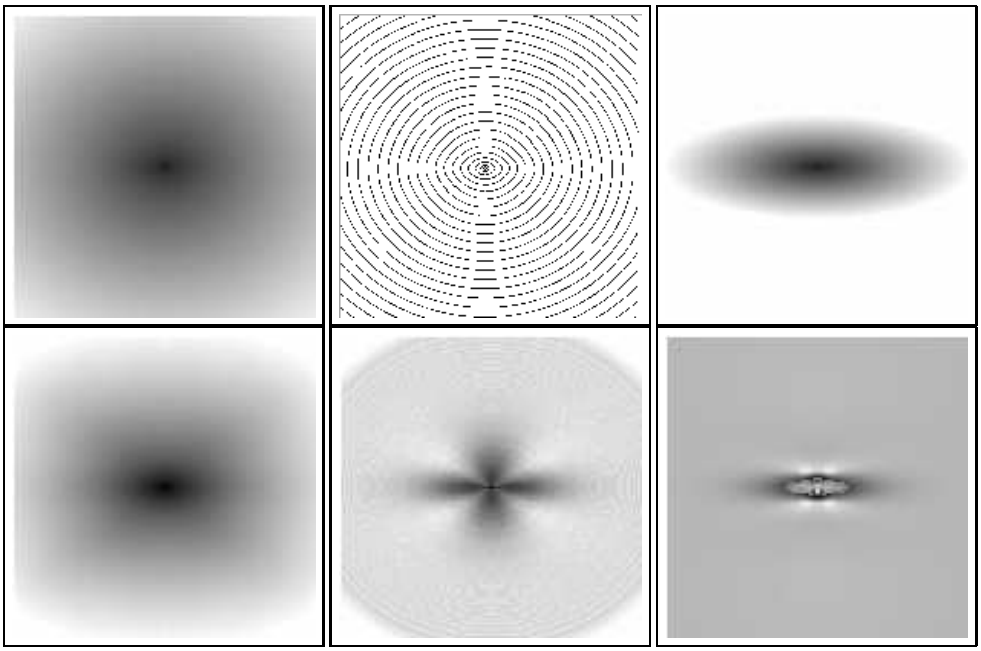

Fig. 11 As Fig.9 but for model **DBNI**$_2$.

4.2 Methods to visualize the inner structure

We apply four different techniques to visualize the substructure in the inner region ($\lesssim$ 1 kpc) of NGC 3384. The first three methods are based on the idea of a galaxy composed of large-scale regular components (the "underlying galaxy" = disk + bulge) hosting additional, smaller-scale components; the methods try to separate the latter. The last method is based on the Laplacian pattern enhancement operator. The methods were amply tested by simulated images (see below).

- *Profile decomposition*

The decomposition of the surface brightness profile is a conventional technique to characterize the basic components of a galaxy. For NGC 3384, however, the decomposition is difficult at larger scales due to the presence of the lense component (at $\sim 35'' \ldots 170''$ along the major axis) and the outer disturbances (Busarello et al 1996). At the scale of the HST images, however, the profile appears to be the composite of essentially three components: the nucleus, the IC and an approximately exponential component ($I \propto \exp\{-r/r_0\}$, where I is the intensity per surface unit and r_0 is the scalelength) which dominates at $a \gtrsim 5''$ (Fig. 12). We use the results from the ellipse fitting (MIDAS procedure FIT/ELL3 in the context SURFPHOT) to build a model image of this exponential component, assuming that it can be extrapolated from the interval $a = 6 \ldots 10''$ to the innermost region. The subtraction of the model from the original image clearly shows the IC (Fig. 6), though the details of the residual image depend on the assumptions on the ellipticity of the inner isophotes of the *underlying* (exponential) component, which cannot be extrapolated with confidence. The residual image in Fig. 6 is for the case that the ellipticity of the underlying component is identical with the ellipticity found from the ellipse fitting procedure.

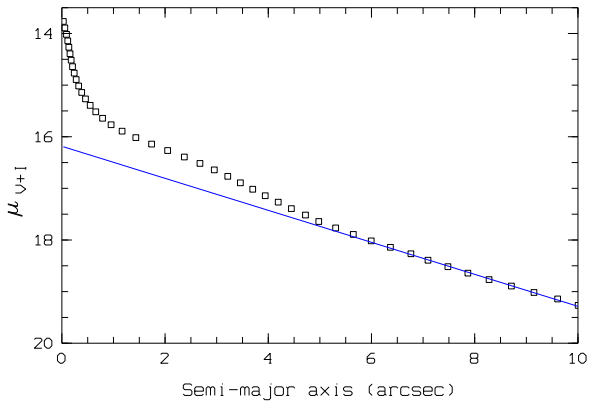

Fig. 12 Surface brightness of the combined *HST* WFPC2 F555W+F814W image as a function of the semi-major axis a (symbols) and the linear regression for $a > 6''$ (line).

- *Unsharp masking*

This method is useful to enhance sharp features on a smooth background by subtracting (or dividing) a smoothed version of an image from (by) the original (e.g., Malin & Carter 1983; Peng et al 2002). We created a blurred image by repeatedly applying a median filter. Prior to the filtering, the pixel values in the central $1''$ were replaced by the values of the neighbour pixels to reduce the effects produced by smearing the bright nucleus. Finally, the median-filtered image was subtracted from the original image. The results depend on the filter size. The residuals from the WFPC2 image are displayed in Fig. 6 for a $2'' \times 2''$ filter, those from the ACS images in the three filter bands are shown in Fig. 7 for the same filter size.

- *Ellipse fitting*

This method is also based on the idea that the underlying extended (outer) galaxy components can be fitted by purely elliptical isophotes. Hence, additional (inner) structures of smaller scales are believed to be extracted by subtracting an ellipse fitting model from the original image. This method was often applied to analyze galaxy components; for a recent example see e.g. Beaton et al (2006).

However, when applied to the original image, the best fitting model is determined not only by the underlying components but, of course, also by the additional components. One solution would be masking of the expected additional structure and computing the ellipse model from the masked image (e.g., Lauer 1985; Busarello et al 1996). Here, we use a different approach based only on the analysis of the isophotes. The basic idea is that any additional light-emitting component yields a corresponding *outward* distortion of the isophote within the angular interval covered by this component. (Analogously, an absorbing component, like a dust lane, produces an corresponding inward distortion.) If the underlying and the additional component differ in ellipticity and/or position angle, the observed isophotes can be subdivided into sections dominated by (A) the underlying components and (B) the underlying+additional components. The ellipse fitting has to be done in the A-sections only. The principle remains the same when two additional components (here: IC and EC) are superimposed as is illustrated by Fig. 4. It is immediately clear that the subtraction of a model image from simple ellipse fitting yields a positive difference in the B-sections and a negative in the A-sections. The result is the well-known appearance of a Maltese cross absorption feature in the residual image (see e.g. Beaton et al 2006; their Fig. 2). The method applied here is aimed at an ellipse model which fits to the isophotes in the A-sections only (IEF = "inner ellipse fitting"): for each intensity level the isophote is compared with a set of fitting ellipses of different size. The size is the free parameter of the fit, the other parameters are taken from the mean fitting ellipse from the FIT/ELL3 procedure.

Of course, the method can work only when the isophotes show obvious deviations from pure ellipses. For the inner

part ($a \lesssim 10''$) of NGC 3384, such deviations are not very strong but present. In the inner $\sim 3''$, the isophotes are nearly perfect ellipses, probably because the IC dominates the image structure. Hence, we simply extrapolate the size correction from the intermediate region ($\sim 3'' \ldots 6''$) towards the centre. The final corrected IEF image is displayed in panel (e) of Fig. 6. We note that the simple ellipse fitting (not shown here) of NGC 3384 yields a very pronounced cross-like feature both in emission and absorption. This feature is considerably reduced by the IEF method and the subsequent size correction but does not disappear completely.

- Adaptive Laplace filtering

Finally, we processed the WFPC2 image through an adaptive Laplacian filter. Laplace filtering uses the second derevatives of the image and is therefore a useful tool of structure recognition; adaptive filtering means to look for the spatial frequency band containing the relevant signal and to enhance particularly the structure in this band (e.g. Richter et al 1991). Adaptive Laplacian filtering has been successfully applied by Busarello et al (1996) and has led to the discovery of the IC. Here we applied the MIDAS procedure FILTER/ADAPTIVE with the Laplace filter where the parameters were chosen after extensive tests (pyramidal impulse response with a maximum size of 95, a significance threshold of $k = 3$, and an assumed Poisson noise). The result is shown in panel (f) of Fig. 6. We performed extensive modelling to understand the structures in this image (see below).

4.3 Tests with simulated galaxies

Here we describe synthesized images from simulated galaxies which were analyzed in the same way as the *HST* images of NGC 3384. The aim is to provide a better understanding for the structures revealed and/or produced by the image analysis techniques. It should be explicitely pointed out that it is not the intention of this section to search for a kind of "best fit" models.

In general, the models consist of five components: (a) the extended, inclined galaxy disk, (b) a bulge, (c) a compact central component, called "nucleus", (d) an inner component, called IC, which is elongated in the same direction as the projected disk, and (e) an elongated inner component, called EC, stretching perpendicular to the IC. The model images were constructed using the MIDAS procedure CREATE/IMAGE with an usual exponential law for a thin, face-on galaxy disk, an $r^{1/4}$-law for an spherical-symmetrical bulge, and a Gaussian with $\sigma_{\rm x,y} = 1\,$px for an unresolved nucleus. For the IC we adopt an inclined exponential disk at $PA = 90^\circ$ with a scale length between 0.02 and 0.1 of that of the extended galaxy disk. The EC is represented by an extended, elongated component at $PA = 0^\circ$ with a surface brightness distribution following an $r^{1/4}$-law, though other luminosity profiles were simulated as well. The inclination of the IC is varied between $i = 80^\circ$ and 60° (less inclined disks become photometrically undetectable; Rix & White 1990) where i is the angle between the line of sight and the direction perpendicular to the plane of the IC. All components are co-centric. For four realizations the synthesized images are displayed in Figs. 8 to 11 along with the results from the image processing. The intensity levels in the contour plots are equal-spaced with steps of $\Delta \log I = 0.1$. The models are listed in Table 1. Disk, bulge, and nucleus have the same parameters in all displayed images. Model DBN is used only to check for numerical artifacts from the image analysis. The comparison of Figs. 9 and 10 allows to evaluate to effect of an EC-like component and the comparison of Fig. 10 with Fig. 11 illustrates the effect of changing the inclination of the IC. The extracted structures from the image analysis can be compared directly with the images of the corresponding input components. The additional components are clearly recognized in the results from all methods, but it is also obvious that all methods produce deformations or "artifacts".

Table 1 Simulated galaxies from Fig.s 8 to 11

model	components
DBN	disk, bulge, nucleus
DBNEI$_1$	disk, bulge, nucleus, EC, IC ($i = 80^\circ$)
DBNI$_1$	disk, bulge, nucleus, IC ($i = 80^\circ$)
DBNI$_2$	disk, bulge, nucleus, IC ($i = 70^\circ$)

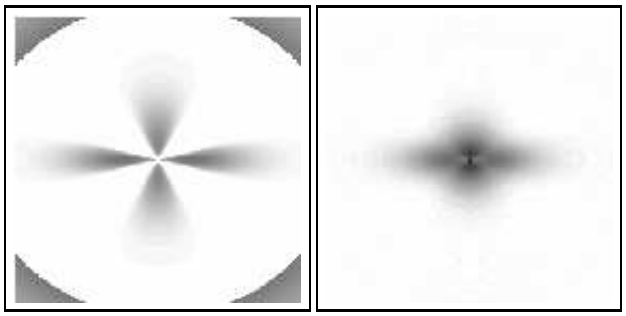

Fig. 13 Comparison of the residual image from the simple ellipse fitting (left) and the corrected IEF (right) for the same model (DBNI$_1$).

The unsharp masking provides a good impression of the basic structure of the components, but the underlying components are still very prominent. The residuals from the subtraction of corrected IEF models are contaminated by effects due to the discrete step size of the intensity of the fitting ellipses especially in the outer regions. In the inner region, the well-known Maltese cross is produced (Fig. 10). Compared to the residual image from the simple ellipse fitting, the Maltese feature is substantially suppressed in the corrected IEF image (Fig. 13). However, it does never dis-

appear completely, even in the model galaxies without EC (Figs. 10 and 11). The reason is that the method works only as long as the isophotes clearly deviate from pure ellipses, as mentioned already in Sect. 4.2. For small deviations, the A- and B-sections (Fig. 4; Sect. 4.2) are not precisely enough defined. This is the case when the additional components have a similar shape and orientation as the underlying components, as is illustrated by the comparison of Figs. 10 and 11: the galaxy models are the same with the only difference in the inclination of the IC. Because of the lower inclination in Fig. 11, the underlying component and the additional component (IC) show less significant differences and the isophotes of the model galaxy hence show smaller deviations from pure ellipses. Due to the assumed symmetry, small systematical errors in the determination of the A- and B-sections produce cross-like structures. This can result also, of course, in apparent absorption features, even though the method of the *inner* ellipse fitting was constructed to avoid such artificial structures.

Finally, the Laplace filtering yields noticeable signals at positions where the intensity gradient abruptly changes. The filtered images allow to estimate the structure and also the size of the inner components. In particular, there are strong negative signals at either side as well of the IC as of the nucleus parallel to IC's major axis. At somewhat larger distance from the centre, two extended side-lobes appear in the direction of the EC in models where there is no EC. Theses features are very faint and are not clearly recognizable on the reproductions in Figs. 10 and 11

4.4 Results

The results from the combined WFPC2 image are summarized in Fig. 6. The IC is clearly indicated in the final images from all four image processing techniques. The residual images from the profile decomposition and from the unsharp masking (both are reproduced with high contrast) reveal an ellipsoidal structure at P.A.$= 46^\circ$ with a maximum semi-major axis of $\sim 5 \ldots 6''$. This is consistent with the structures seen in the images from the ellipse fitting procedure and the Laplace filtering (compare Figs. 6 and 11). The Laplace filtered image indicates, in addition, a minimum in the radial change of the slope of the radial profile along the major axis at about $2''$ from the centre, indicating that the profile of the IC becomes shallower towards the centre. This characteristics becomes directly visible in Fig. 14 where the surface brightness profile of the residual component is shown after subtraction of the model from the profile decomposition. Obviously, the radial intensity profile of the IC is not adequately described by the usual exponential law of stellar galactic (outer) disks. Below $\sim 1''$, the surface brightness increases rapidly towards the centre.

On the unprocessed *HST* images, the maximum ellipticity of the IC is $\epsilon_{\max,\mathrm{IC}} = 0.44$ (Fig. 5). Busarello et al. (their Fig. 4) give smaller values of ~ 0.4 for the NTT image and ~ 0.3 for the other images. The corresponding value from our Calar Alto data is ~ 0.35, in good agreement with Busarello et al. Because these differences are obviously a resolution effect, the best value is that from the *HST* observations. The measured ellipticity is expected to be affected also by the profile of the underlying galaxy. After subtraction of the model from the profile decomposition we measure indeed a higher value of $\epsilon_{\max,\mathrm{IC}} = 0.50$ (Fig. 14). If the ellipticity is interpreted as due to an inclined disk, the IC has nearly the same inclination as the outer disk ($\epsilon_{50} = 0.49$; see Sect. 3). The position angles, however, are slightly different: 46° for the IC and 51° for the outer disk.

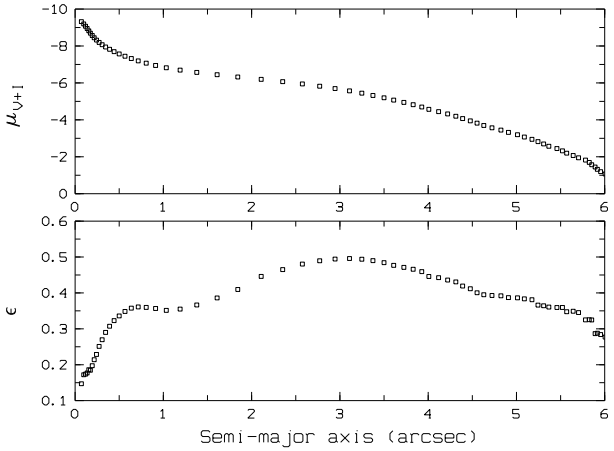

Fig. 14 Surface brightness μ and ellipticity ϵ of the residual WFPC2 image after subtraction of the model image from profil decomposition.

The EC is weakly indicated in all images, also in the Laplace filtered image (though it is not visible in the reproduction in Fig. 6 where the intensity cuts were chosen to visualize the structure of the IC). Our images corroborate the earlier finding (Busarello et al 1996; Sil'chenko et al 2003) that the elongation of the EC is nearly perpendicular to the IC. There is no indication for inner structure in the EC. However, we find that the contribution of the EC to the total intensity per surface unit does not exceed 8%, while Busarello et al report a maximum of 15% at larger distances from the centre. This is in agreement with the visual impression that the relative strength of the EC has its maximum at $\sim 15''$ from the centre and is much fainter inside. We notice that such a behaviour is not reproduced by the bars in our simulations.

The residuals from the subtraction of the median filtered images in three filter bands of the *HST* ACS images are shown in Fig.7 along with the corresponding contour plots. The intensity levels in the contour plots are equal-spaced with steps of $\Delta \log\, I = 0.1$. At longer wavelengths (F555W; see also the combined image in Fig. 6), the IC is traced out to distances of about $4\farcs5 \ldots 5\farcs5$ (about 250 ... 300 pc). From the comparison of the residual images from the profile decomposition with the original images, we estimate that the surface intensity of the IC on the major axis at

$a \approx 3''$ is probably as high as 30 to 40 per cent of the galaxy (see also Figs. 5 and 12). This is clearly at variance with the upper limit of 5% estimated by Busarello et al. The most likely reason for this discrepancy is the higher resolution of the *HST* images.

The centre of NGC 3384, and also the IC, are clearly detected at 2500Å (Fig. 7). This UV background appears to be caused mainly by low-mass, helium-burning stars in the horizontal branch and subsequent phases of evolution (see O'Connell 1999). An important consequence is that the UV background allows to detect efficiently faint dust extinction features (see Sect. 6).

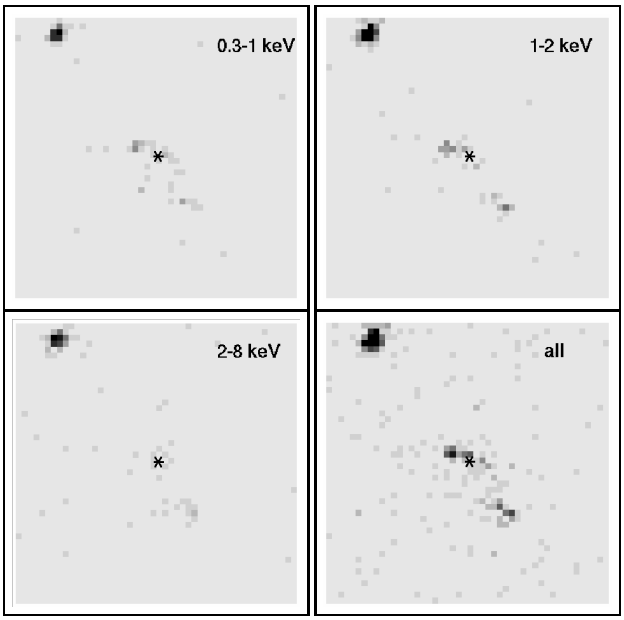

Fig. 15 *CHANDRA* image of the inner 24″of NGC 3384 (same scale as in Fig. 6). The position of the optical centre of the galaxy is marked by the black asterisk in the image centre.

Finally, the *CHANDRA* image of NGC 3384 is worth noticing (Fig. 15). There are three, perhaps four or five, fainter X-ray sources in the image and a brighter source at the NE corner. One source is close to the centre of the galaxy, though presumably not identical with the nucleus. The position of the optical centre was determined by five X-ray sources in the whole *CHANDRA* field which were unambiguously identified with optical sources. NGC 3384 is "X-ray faint" in the sense that it is devoid of a large gaseous X-ray halo. In X-ray faint early-type galaxies, low-mass X-ray binaries (LMXBs) are known to account for a large fraction of the total X-ray emission (Fabbiano 2006). Hence, it is tempting to speculate that the sources seen in Fig. 15 are mostly LMXBs; a more detailed discussion is beyond the scope of this paper. Here, we just notice that the distribution of the X-ray sources shows approximately the same orientation as the IC.

5 Age estimation

An excellent analysis of the ages of the stellar population in the centres of the three brightest Leo I galaxies, NGC 3368, NGC 3379, and NGC 3384, has been presented by Sil'chenko et al 2003. Based upon Lick indices from integral field spectroscopy, they discovered separate circumnuclear subsystems in all three galaxies. In the centre of NGC 3384, a chemically distinct subsystem was found with an age of about 3 Gyr, a super-solar metallicity $Z \approx 0.04$ ([m/H] = 0.35) and an overabundance of α elements ([Mg/H] ≈ 0.3). The extent of this component was found to be comparable to or smaller then the resolution limit of $\sim 1''$. In the nearest vicinity of the nucleus, the metallicity and the relative abundances drop to solar values while the mean age increases to 7-8 Gyr. The use of the spectroscopic Lick indices provides the advantage of being widely unaffected by dust. On the other hand, the limited field of view of integral field spectrographs can be a drawback sometimes. For the investigation of the stellar population on larger scales in nearby galaxies, the multi-colour photometry hence remains an important tool.

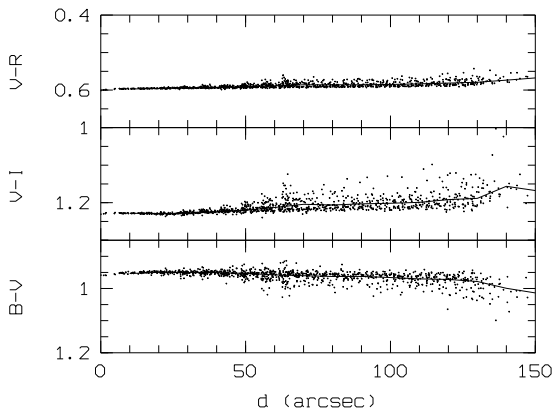

Fig. 16 The colours for points located along or parallel to the major axis versus distance d from the centre. The solid lines are running means.

Here we use our multi-colour photometry on the Calar Alto images to quantify characteristics of the large-scale distribution of stellar populations in NGC 3384 by the comparison with model colours. Colour indices were measured in scans parallel to the major axis of the galaxy and parallel its the minor axis, respectively. Measurement apertures of $1''$to $2\farcs5$ diameter were used separated by $2\farcs5$. The measurements for the scans parallel to the major axis are shown in Fig. 16, the results for the scans parallel to the minor axis are very similar. We conclude that the colours do not significantly vary with position on large scales, in agreement with Busarello et al. In particular, there are no significant systematic large-scale colour gradients. The mean values ($\pm 1\sigma$ uncertainties) of the colour indices are $(B-V, V-R, V-I) =$

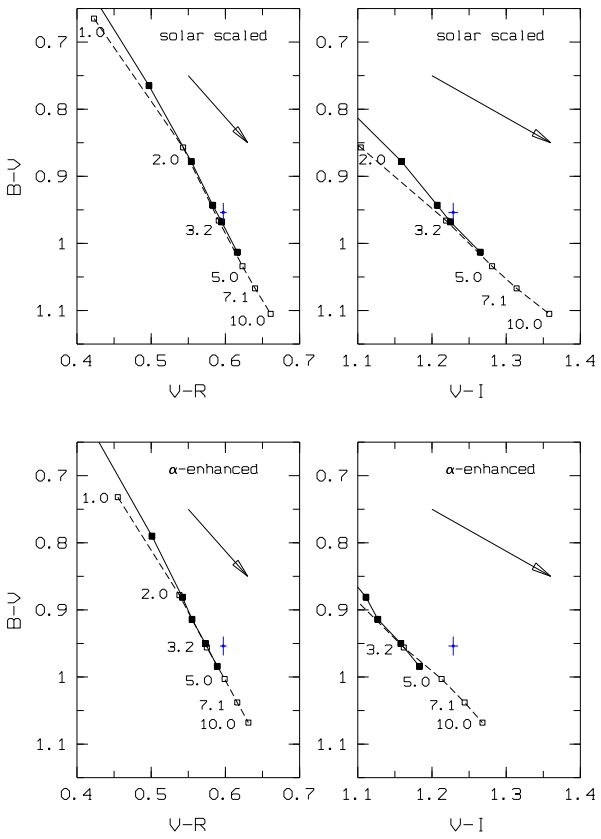

Fig. 17 Colour-colour diagrams with evolutionary tracks of single starburst populations with solar-scaled (top) and α-enhanced (bottom) relative abundances from Salasnich et al (2000) for metallicity $Z = 0.019$ (solid line, filled squares) and $Z = 0.04$ (dashed line, open squares), respectively. The points along the tracks correspond to ages of 10.0,7.1,5.0,3.2,2.0, and 1.0 Gyr (bottom to top; the youngest model points are beyond the boundaries for some tracks; for lucidity only the age points on the super-solar metallicity tracks are labelled). The mean colours of the stellar population in NGC 3384 are marked by the small dot with 1σ error bars. The arrows are the reddening vectors for standard Galactic dust and $E(B-V) = 0.1$ mag.

$(0.954\pm0.014, 0.597\pm0.045, 1.229\pm0.065)$. In Fig. 17, we compare the mean colour indices with the synthetical stellar population models from Salasnich et al (2000). We conclude that the dominant stellar population in NGC 3384 has an age of about 5 to 7 Gyr and approximately solar metallicity, in good agreement with the results from Sil'chenko et al.

It was actually one of the primary aims of our multi-colour photometry to look for large-scale variations of the dominant stellar population. Expected colour differences can be estimated by the comparison of the results from Sil'chenko et al for the nucleus and the host galaxy with the population synthesis models from Salasnich et al. In the terminology of the models, the nucleus corresponds to 3 Gyr, $Z = 0.04$, and α-enhanced abundances, the main body of the galaxy corresponds to 7 Gyr, $Z = 0.019$, and solar-scaled abundances. The colour differences of the two corresponding model points are $(\Delta(B-V), \Delta(V-R), \Delta(R-I)) = (0.012, 0.020, 0.063)$, i.e. very small.

Let us now assume that the EC and the IC are made up of the same stellar population as the nucleus. In that case, the colour difference between the host galaxy and the areas covered by these components is even smaller because they contribute only a fraction to the total light: $\leq 15\%$ for the EC (Busarello et al 1996) and $\lesssim 40\%$ for the IC (Sect. 4). From these values one easily estimates a colour difference relative to the underlying galaxy of $\Delta(B-V) < 0.002$ mag for the EC and less than 0.005 mag for the IC, too small to be clearly detectable. Hence, our photometry does not allow to decide whether the formation of the EC and IC is related to the same event in the evolution of NGC 3384 which triggered the starburst in the nucleus.

We explicitely note that it was not our intention to measure colour gradients very close to the centre. The positions of the measurement apertures were not selected with special consideration of colour changes within the innermost few arcseconds. Systematic reddening in the nearest vicinity of the nucleus has been reported already in several studies done with higher resolution (Busarello et al 1996; Sil'chenko et al 2003; Lauer et al. 2005). Some of these colour values have to be taken with care since the images were not accurately calibrated (including in particular $U-V$ in Fig. 5 of the present paper, but also $V-I$ in Lauer et al, and the V magnitudes in Busarello et al). The $B-V$ colour profiles shown by Busarello et al indicate a colour difference of $B-V \approx 0.10 \ldots 0.15$ mag between their innermost point at $a = 1''$ and the region at $\gtrsim 2''$ along the minor axis and $\gtrsim 5''$ along the major axis, respectively. Along the major axis, most of the reddening appears to be within the innermost $\sim 2''$. The higher resolution of the *HST* images indicates that the reddening is probably even stronger concentrated toward the nucleus.

6 Discussion: the dust in the central region of NGC 3384

With the ages and metallicities from the spectroscopic Lick indices for (a) the nucleus and (b) the rest of the galaxy, on the one hand, and the good agreement of these data with our mean colours, on the other hand, the colour gradients close to the nucleus remain to be explained. From Fig. 17, it is immediately clear that a reddening of about $E(B-V) \approx 0.1 \ldots 0.2$ mag toward the nucleus cannot be due to the change in the stellar population. A reasonable assumption is reddening due to dust. The issue of dust in the centre of NGC 3384 will be discussed in detail below.

The possibility that dust lanes are common to early type galaxies was discussed already by Lauer (1985). The high-resolution of the *HST* images allows to detect small-scale dust extinction features. It is well known from such studies that dust features are common in the central regions

of early-type galaxies. In the sample of nearby early-type galaxies studied by Lauer et al (2005), dust is visible in 47% of the 177 galaxies. No dust obscuration was found in NGC 3384 on the WFPC2 images (Tomita et al 2000; Lauer et al 2005). The surface brightness distribution appears smooth also on the unsharpe masked ACS F555 and F330 images in Fig. 7. However, dust absorption features are detectable best in the UV due to the high selective UV extinction. The ACS F250W image indicates some faint fuzzy structures, most discernible on the contour plot. If these structures are due to dust, e.g. a faint dust lane related to the EC, the *maximum* local extinction is estimated to $A_{\lambda 2500} \sim 0.5$ mag, corresponding to $E(B-V) \leq 0.07$ mag for standard Galactic dust. The colour index $U-V$ (Fig.5) seems to be slightly (~ 0.05 mag) enhanced in the middle of the IC ($a \approx 2 \ldots 3''$) and is increasing towards the nucleus at $a \lesssim 1''$.

Can we exclude additional reddening due to a smoothly distributed dust component? In order to answer this question, we estimate the dust extinction from the amount of cool gas. Early-type galaxies are known to have only a low fraction of mass in cool interstellar matter (ISM). Moreover, the measured gas masses in S0 galaxies are even less than 10% of the masses expected to be returned to the ISM by evolved stars over a Hubble-time, $t_{\rm H}$. Gas masses of a sample of 27 nearby S0 galaxies, including NGC 3384, were derived by Sage & Welch (2006). With a total mass of $5\,10^6 {\rm m}_\odot$ for the cool ISM (neutral and molecular gas), NGC 3384 is among the most gas-poor galaxies in this sample. Nevertheless, dust can have an effect if it is strongly concentrated. Many galaxies have peak CO emission in the centre (Regan et al 2001; Helfer et al 2003) and molecular gas is known to be more centrally concentrated in galaxies with bars (Seth et al 2005). For the most gas-poor S0 galaxies studied by Sage & Welch, the cool gas is dominated by the molecular phase which seems to be concentrated towards the galaxy centres while the neutral gas is probably more widely distributed (Sage & Welch 2006). A median size of the CO-emitting region of 0.7 kpc has been derived by Welch & Sage (2003). This corresponds to $12''$ for NGC 3384, if we assume the distance of 8.1 Mpc used by these authors, and scales to 1.0 kpc for the distance used here. From the observed gas mass in this volume, we estimate the effect of dust assuming that (1.) the ISM in the central part of NGC 3384 is completely dominated by the molecular gas, (2.) the molecular gas is located completely within the inner 1 kpc, (3.) the dust-to-gas mass ratio corresponds to the standard value of 0.01, (4.) the dust density is independent of position, and (5.) the dust acts as an extinction screen. For the standard Galactic extinction curve we find $A_{\rm V} \approx 0.3$ mag and $E(B-V) \approx 0.1$ mag for the centre of NGC 3384.

As a consistency check, we compare the estimated dust mass with the IRAS data. From the IRAS SCANPI data we find a 12 μm flux density of $f_{12} = 0.13$ Jy, but no signal at longer wavelengths. This does not fit the spectral energy distribution of dust at a typical temperature of $T_D \approx 30$ K (assuming the usual λ^{-1} emissivity law), which obviously means that the 12 micron flux is not dominated by the cool interstellar dust (in agreement with the IRAS data from other S0 galaxies; see Soifer et al 1987, and references therein). Using the relation between dust mass, infrared luminosity, and T_D given by Soifer et al (their eq. 1), we derive flux densities which are below the IRAS limit for $T_D < 40$ K. Hence, the IRAS upper limits for $\lambda > 12\,\mu$m do not contradict to the estimated dust mass as an upper limit. A substantial fraction of the dust in a warm phase at $T \approx 200$ K, as was found e.g. in the centre of the S0 galaxy NGC 3998 (Knapp et al 1996), can be excluded for NGC 3384.

We emphasize that the above estimate of dust reddening is relatively uncertain. In particular, a correction is obviously required with regard to assumption (5): the dust obscures only the light sources that are behind it and not the stars between the dust and the observer. Moreover, the estimated values are further reduced by a factor of ~ 3 if we identify the size of the CO-emitting region in NGC 3384 with the beam size of the observations ($21''$ FWHM) rather than the median value of the galaxy sample.

A more fundamental question arises from the facts that dust (1.) is expected to be present as a consequence of the evolution of the stellar population and (2.) should be related to the amount of cool gas, namely: why is NGC 3384 that dust-poor? An explanation for the under-abundance of dust in S0 galaxies was proposed by Lauer et al (2005). According to their scenario, dust appears at times throughout the galaxy and then falls to the centre where it is being processed or destroyed e.g., due to sputtering by hot X-ray gas. This assumption of episodic dust settling implies that dust is appearing and disappearing continually in early-type galaxies i.e., dust-free galaxies represent the end of a natural cycle where galaxies with lots of dust represent the other end. The length of the dust-free phase was estimated by Lauer et al to be on the order of a few times 10^7 yr and the length of the whole cycle is only 10^8 yr, i.e. much shorter than the timescale for the infall of gas from the outer parts of the galaxy or from outside. Though this concept of a dust settling sequence appears attractive, a clear idea of the main driver of the cycle is still lacking, as was pointed out already by Lauer et al.

Assuming the majority of the dust in the centre of NGC 3384 has been processed/destroyed, the question remains why molecular gas is detected there. If (1.) the dust cycle represents a cycle of accretion of matter by the central black hole and (2.) nuclear activity is signified by optical line emission – as assumed by Lauer et al – NGC 3384 must be in a post-activity phase. Assuming that the cool ISM has been completely destroyed in the activity phase, by either the accretion onto or the feedback from the nuclear black hole, it can consist now only of the material returned by evolved stars during the dust-free phase of the cycle. Since the timescale of this phase is about $10^{-3}\,t_{\rm H}$,

the mass of the cool ISM is expected to be $\lesssim 10^{-3}$ times the mass returned during $t_{\rm H}$. This is indeed consistent with what was found for the most gas-poor S0 galaxies by Sage & Welch (2006). To check this idea further, we searched for a correlation between the relative (i.e., observed *versus* predicted) gas mass and the presence of dust in the centres of S0 galaxies. Unfortunately, there is no much overlap between the Welch & Sage sample and the Lauer et al sample. Among the six galaxies which are in both samples, five have measurements of the gas mass, two of them show dust obscuration (NGC 3607 and NGC 4026). For the ratio of the observed gas mass to the estimated gas mass returned by evolved stars over $t_{\rm H}$, the mean value for the dust-free galaxies is 10^{-3}, compared to 0.035 for the dusty galaxies. This seems to indicate, that dust-poor S0 galaxies indeed represent the phase of a generally reduced cool ISM. The statistics is however too poor to draw stringent conclusions. In the present context, we conclude that the estimated small dust reddening from the gas mass is at least not at variance with the scenario of the dust settling cycle.

To summarize this discussion, we conclude that NGC 3384 is likely in the dust-poor phase of the dust-settling cycle. Nevertheless, dust reddening by $E(B-V) \approx 0.1$ mag is not implausible in the central region of NGC 3384, though there is no direct clear-cut observational evidence.

7 Conclusions

Based on *HST* archive images we were able to confirm the compact inner component (IC) in the centre of NGC 3384. This peculiar structure, discovered by Busarello et al (1996) on a Laplace-filtered NTT image, was hitherto not seen on direct images. We visualize the IC using various methods of image processing. The images show also the extension of the well-known bar-like elongated component (EC) toward the centre of the galaxy. For the IC, our results confirm the previously estimated maximum semi-major axis of $5 \ldots 6''(\sim 300\,{\rm pc})$ and the position angle $PA \approx 46°$. The superb resolution of the *HST* images allows a better determination of the shape and the relative light contribution. The IC is found to contribute up to ∼40% i.e., a factor of ∼8 higher than estimated by Busarello et al. For the EC, on the other hand, we estimate a slightly lower fraction than Busarello et al. This is in agreement with the visual impression of the well-known peanut-shape because the maximum relative contribution of the EC is at larger distances, out of the *HST* field. The maximum ellipticity of $\epsilon_{\rm max,IC} \approx 0.5$ is higher than determined in previous studies and signifies the same inclination as the outer disk. The disk-like structure of the IC seems to support the interpretation as an inner disk which is in line with the kinematical data from two-dimensional spectroscopy (Busarello et al 1996; Fisher 1997; Sil'chenko et al 2003; Emsellem et al 2004). The intensity profile of the IC is not well approximated by a usual exponential law but becomes shallower toward the centre.

Our broad-band colour indices from Calar Alto images are shown to be in agreement with model predictions for a 5 to 7 Gyr old stellar population of quasi-solar metallicity. No significant large-scale variations of the colour indices over the main body of the galaxy are found. Based on the population synthesis models from Salasnich et al (2000), we discuss the expected colour differences between the EC/IC and the host galaxy. We find that it is not possible, based on our colour measurements, to discriminate between scenarios where galaxy components were made of the same young stellar population as the nucleus or by the older population of the host galaxy. The previously reported colour gradients close to the nucleus are most plausibly explained by small amounts of dust strongly concentrated to the centre, although NGC 3384 appears to have, all in all, a very low dust fraction. According to the episodic dust settling scenario suggested by Lauer et al (2005), the low dust fraction is supposed to be an indication that NGC 3384 is in a post-activity phase and at the beginning of a new dust-settling cycle.

Acknowledgements. H. Ismail is very grateful to TLS for kind hospitality and to the Deutsche Forschungsgemeinschaft for financial support. Part of this work has been done using the *HST* data from the data archive at the Space Telescope Science Institute and data from the *Chandra* Data Archive. STScI is operated by the Association of Universities for Research in Astronomy, Inc., under NASA contract NAS 5-26555. The *Chandra* Data Archive is part of the *Chandra* X-Ray Observatory Science Center which is operated for NASA by the Smithsonian Astrophysical Observatory.

References

Barbon, R., Benacchio, L., Capaccioli, M., 1976, A&A 51, 25
Beaton, R. L., Majewski S. R., Guhatakurta, P., et al 2006, ApJ, submitted (astro-ph/0605239)
Burkert, A., Brodie, J., Larsen, S., 2005, ApJ 628, 231
Busarello, G., Capaccioli, M., D'Onofrio, et al, 1996, A&A, 314, 32
Emsellem, E., Cappellari, M., Peletier, R. F., et al, 2004, MNRAS 352, 721
Erwin, P., 2004, A&A 415, 941
Fabbiano, G., 2006, ARA&A 44, 323
Fisher, D., 1997; AJ 113, 950
Helfer, T. T., Thornley, M. D., Regan, M. W., et al, 2003, ApJS 145, 259
Lauer, T. R., 1985, MNRAS 216, 429
Lauer, T. R., et al., 1995, AJ 110, 2622
Lauer, T. R., Faber, S. M., Gebhardt, K., et al, 2005, AJ 129, 2138
Knapp, G. R., Rupen, M. P., Fich, M., et al, 1996, A&A 315, 75
Kormendy, J. & Richstone, D., 1995, ARA&A 33, 581
Kormendy, J. & Kennicutt, R. C., 2004, ARA&A 42, 603
Malin, D. F., 1984, in: Astronomy with Schmidt Type Telescopes. IAU Coll. 58, ed. M. Capaccioli (Reidel: Dordrecht), p. 73
Malin, D. F. & Carter, D., 1983, ApJ 274, 534
O'Connell, R. W. 1999 ARA&A 37,603
Pease, F. G., 1920, ApJ 51, 276
Peng, E. W., Ford, H., C., Freeman, K. C., et al., 2002, AJ 124, 3144

Pinkney, J., Gebhardt, K., Bender, R., et al., 2003, ApJ 596, 903
Prugniel, P. & Heraudeau, P. 1998, A&A Suppl., 128, 229
Regan, M. W., Thornley, M. D., Helfer, T. T., et al, 2001, ApJ 561, 218
Richter, G. M., Böhm, P., Lorenz, H., et al, 1991, Astron. Nachr. 312, 345
Rix, H.-W., & White, S. D. M., 1990, ApJ 362, 52
Rood, H. J. & Williams, B. A., 1985, ApJ 288, 535
Sage, L. J. & Welch, G. A., 2006, ApJ 644, 850
Salasnich, B., Girardi, L., Weiss, A., Chiosi, C. 2000 A&A, 361, 1023
Seth, K., Vogel, S. N., Regan, M. W., et al, 2005, ApJ 632, 217
Sil'chenko, O. K., Moiseev, A. V., Afanasiev, V.L., et al, 2003, ApJ, 591, 185
Sil'chenko, O. K., 2006, ApJ 641, 229
Soifer, B. T., Houck, J. R., Neugebauer, G., 1987, ARA&A 25, 187
Tomita, A., Aoki, K., Watanabe, M., et al, 2000, AJ 120, 123
Tonry, J. L., Dressler, A., Blakeslee, J. P., et al, 2001, ApJ 546, 681
Toomre, A., Toomre, J. 1972, ApJ, 178, 623
Tremaine, S., Gebhardt, K., Bender, R., et al, 2002, ApJ 574, 740
Welch, G. A. & Sage, L. J., 2003, ApJ 584, 260